

# Dynamics of Complex Fluids

## Part II Physics Experimental Report

November 2017

### Abstract

Particles undergoing Brownian Motion are known to follow certain probabilistic laws. An analysis of light scattered by colloidal particles suspended in fluid undergoing such Brownian Motion was performed using two different techniques: Dynamic Light Scattering and Differential Dynamic Microscopy. From this analysis we were able to determine either fluid or particle properties.

The two techniques and their limitations were compared, in particular for a colloid of diameter  $0.3 \mu\text{m}$  a DLS method gave a value of  $2.1 \pm 0.2 \mu\text{m}$  and DDM  $0.321 \pm 0.003 \mu\text{m}$ . Multiple particles sizes were analysed using DDM and the error was seen to increase with particle size.

The DDM technique was then applied to a variety of viscoelastic fluid/colloid mixtures. Here we were able to find the behaviour of many fluid's Complex Modulus as a function of frequency to within some level of agreement with previous literature. We then examined gravity forced particle motion and were able to accurately extract the terminal falling velocity, except when using heavier beads for which an atypical diffusive behaviour was observed. Finally, a mixture of two colloids was imaged and the diameters of the particles involved were fairly accurately determined, despite analytic setbacks.

DDM has proved itself a powerful successor to DLS, and promises to drive future research in multiple areas.

## 1 Introduction

The thermal energy of particles at room temperature gives rise to a well-documented phenomenon – Brownian Motion. Even systems that seem small on a human scale contain unfathomably large numbers of particles, each of which is constantly moving, colliding and randomising any previously existing structure. Individually a particle may well obey Newton's or Schrodinger's Equation, but any such case by case treatment is doomed to fail simply by sheer weight of numbers. A treatment using statistical averages on the other hand makes use of the very large numbers involved, providing remarkably accurate results as a consequence. Einstein studied Brownian motion, laying the groundwork for its systematic understanding, while also providing convincing evidence of the particulate nature of the world. We shall make extensive use of a textbook result concerning the diffusive behaviour of particles, that the mean squared displacement of particles is linear with time:

$$\langle x^2 \rangle = 2D\tau$$

D is the Diffusion coefficient defined as:

$$D = \frac{k_b T}{\zeta}$$

Where  $\zeta$  is the drag coefficient, a function of both particle size and fluid characteristics such as Reynolds number.

While such diffusive systems are all around us, for the most part the particles involved are very small, on the order of nanometres. They do interact with visible light, the sky is blue for example, but only to a limited degree. By placing larger, micrometre scale, tracers in the fluid we can much more easily visualise the behaviour using optical setups. The equations above can be used to relate particle to fluid properties, allowing us to learn about one using information about the other. In particular, we shall be using spherical beads whose Diffusion Coefficient is given

by the Stokes-Einstein Law, a first order simplification of the Navier-Stokes Equation in the Low Reynolds number regime:

$$D = \frac{k_b T}{6\pi\eta a}$$

Where  $\eta$  is the viscosity of the fluid in which the tracers are placed, and  $a$  is the diameter of the particles.

Light that impinges on our sample will be scattered by these spherical tracers. Each particle will act as a source of secondary Huygen's wavelets. Just like a grating, each spatial frequency present in the particle distribution at a given time will scatter the light at a particular angle. However, in our sample the 'grid' of scattering sources is constantly rearranging and randomising its position. Even using a coherent and monochromatic laser beam we would therefore expect that the scattering due to any one spatial frequency would look more like a noise source. In order to pull meaning from this seemingly unimpressive collection of data we therefore autocorrelate it, an operation defined for a function  $f(t)$  as follows:

$$F(\tau) = \int_{-\infty}^{\infty} f(t + \tau)f(t)dt$$

The resulting function  $F(\tau)$  quantifies the degree of coherence between a signal at one time with that at a lag time  $\tau$  later. At very small  $\tau$  you would expect the autocorrelation to be very large, as the signal will not have had time to change, while at very large lag times the system will be completely randomised and the autocorrelation will plateau. At intermediate times the function can be shown to undergo an exponential decay with decay constant  $\frac{1}{Dq^2}$ , at least for monodisperse samples[1].

As a simplification the characteristic decay time represents a rough estimate of the average time it takes for a particle to travel the wavelength of the particular spatial frequency under consideration. Within this time the particles are able to randomise the pattern present at that spatial frequency and hence decorrelate the measured signal. The factors in this argument are not precise, a more rigorous analysis is presented in Pecora and Berne's book[1].

Thus the above theory allows us to relate the decay constant of the autocorrelation function with spatial frequency. This relationship depends on the diameter of the particle and the viscosity of the fluid allowing us to retrieve this information from our data.

All we need now is a method of collecting this data. We present two in this report; the first is Dynamic Light Scattering (DLS). A summary of the technique and a record of our use of it are presented in section 2. Our second technique is the relatively new Differential Dynamic Microscopy (DDM), this method and our tuning of its parameters are presented in section 3, in addition to a direct comparison of the two. We then used DDM to explore some more uncharted territory and this is described in section 4.

## 2 Dynamic Light Scattering

### 2.1 Theoretical Background

DLS fundamentally consists of directing a coherent monochromatic laser light through fluid laced with tracer particles. Each spatial frequency present in the particle distribution will scatter light at a different angle, just like a grating. By placing our detector at a particular angle we choose one particular spatial frequency,  $q$ , as shown in figure 1. The precise relationship between the angle and  $q$  can be worked out as follows:

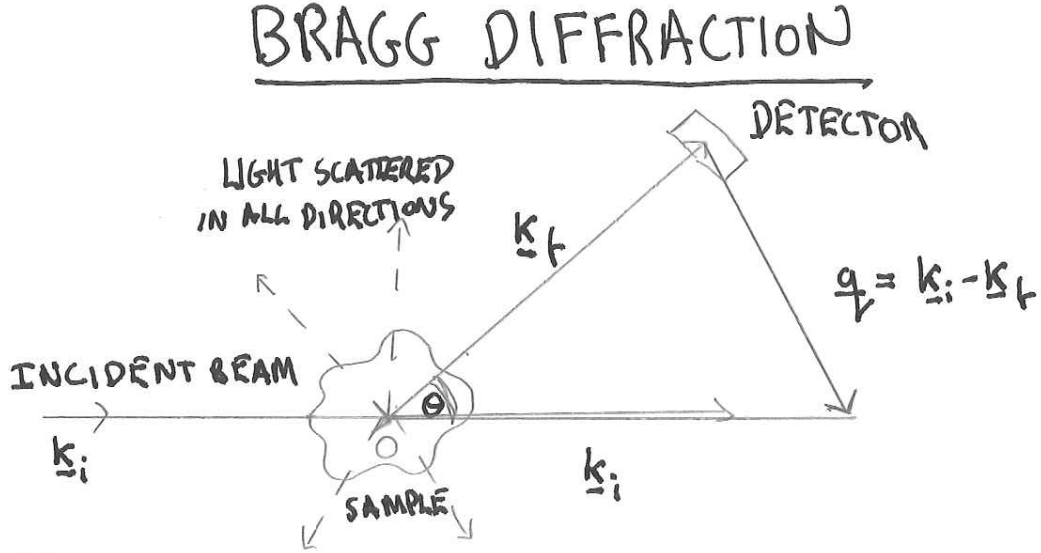


Figure 1: Diagram showing the scattering of a light ray by a spatial frequency  $q$  within the sample. After Berne and Pecora [1].

The cosine law for a triangle allows us to relate:

$$q^2 = K_i^2 + K_f^2 - 2K_i \cdot K_f$$

It is fair to say that the wavelength changes little upon scattering:

$$K_i \approx K_f$$

$$q^2 \approx 4K_i^2(1 - \cos\theta) = 2K_i^2 \sin^2 \frac{\theta}{2}$$

$$q = \frac{4\pi n}{\lambda_i} \sin \frac{\theta}{2}$$

Where  $n$  is the refractive index of the sample,  $\lambda_i$  is the wavelength of incident light and  $\theta$  the scattering angle.

### 2.2 Method and Results

We tested this technique using a sample of fairly homogenous polystyrene beads, diameter  $0.3 \mu\text{m}$ , in water. Of particular interest were the limits of such a technique.

The setup was based around a laser beam,  $\lambda = 635 \text{ nm}$ , and is shown in figure 2. The beam was straightened using a standard mirror setup and then focused onto the sample using a lens. A photodiode was used to measure the intensities at different angles, at a sampling rate of 1000 Hz.

The intensity of the laser was controlled via a polariser. We attempted to minimise background light by placing a black box around the whole setup and turning off all external light sources, however, it still seems that non-negligible light, probably partly reflected laser light, was triggering the detector. We had the laser light intensity at a maximum as the detector measured very little

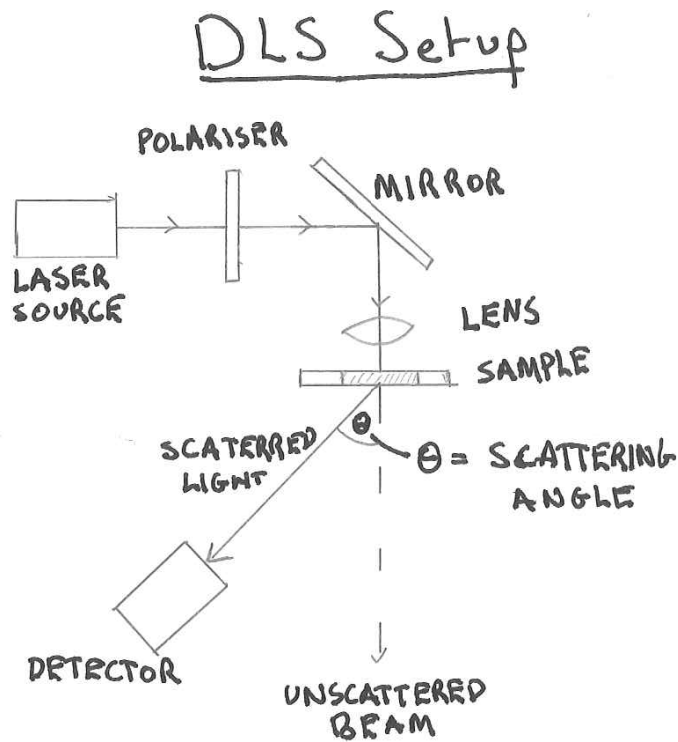


Figure 2: Diagram showing the DLS setup.

signal at almost all angles. This will however have increased the stray laser light at angles close to 0.

A couple of other parameters were tuned. Differing concentrations of colloid did not appear to have a measurable effect in the small range we tested - though of course an opaque sample or equally one with no particles would be useless. On the other hand changing the aperture size allowed more light into the detector and hence produced a larger signal. A large detector aperture would permit a range of angles to enter, introducing error in  $\theta$ , however this error was far smaller than others our analysis produced. More light reaching the detector was, therefore, prioritised and the aperture size was maximised.

We recorded data at a series of different angles between 4 and 90 degrees. An example signal is shown in figure 3. The reading was then autocorrelated, figure 4 shows the autocorrelation of the signal in figure 3. For a short time at the beginning of each recording the autocorrelated signal exponentially decayed as expected, before falling into noise fluctuations. By fitting a straight line to the first few points on a log-log plot of the autocorrelation function we could find the parameters

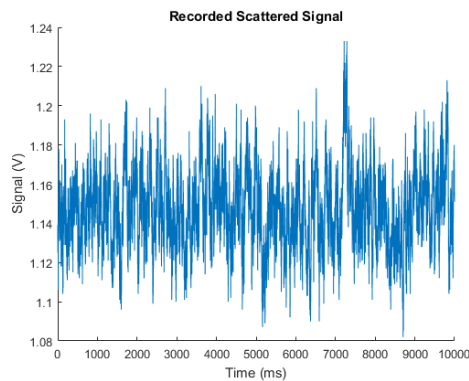


Figure 3: An example of a recorded DLS signal.

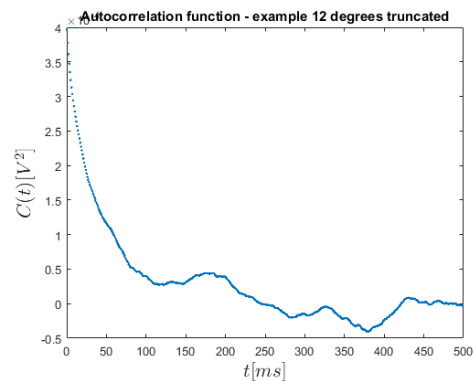


Figure 4: An autocorrelated DLS signal showing exponential decay.

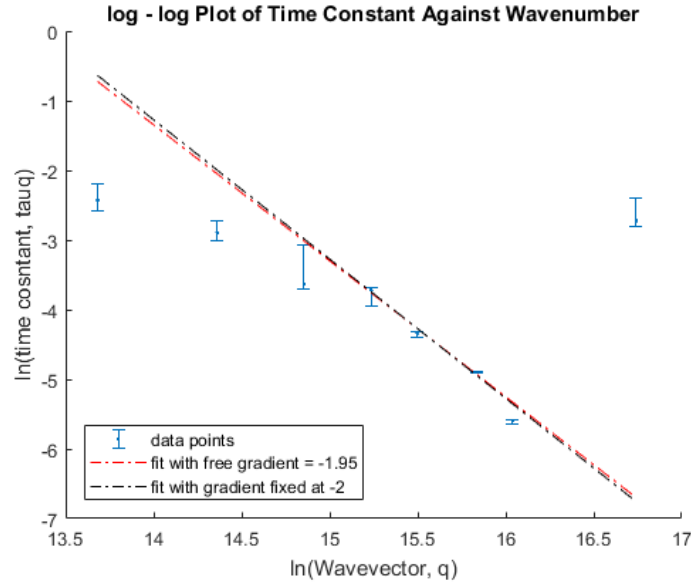


Figure 5: DLS data on log-log plot of time constant against  $q$ . Only the linear region (points 4 to 7) was used for further calculation.

of interest.

In theory the time constant is given by:

$$\tau_c = \frac{1}{Dq^2}$$

So a log-log plot of  $\tau_c$  against  $q$  should produce a straight line with the governing equation:

$$\ln(\tau_c) = -2\ln(q) - \ln(D)$$

Our data is shown in figure 5. There is only a limited linear region in which the equations are being accurately obeyed and it was this region that we fitted to. The figure features two straight line fits; the first with both parameters free has a gradient of -1.95, roughly equal to the theoretical value of -2. The second has a fixed gradient of -2 and this line's intercept was used to calculate  $D$ , and hence the diameter of the particles.

The major source of error on each data point was choosing the number of points from which to calculate a time constant. The decay that was fitted to the autocorrelation function was only fitted to the first few points, as after small times differences the signal became mostly noise (figure 4). However it was hard to determine at which point the noise, rather than the decay, was the most prominent effect, and hence the region over which to perform the fit. It is this variation that the error bars represent. By finding a separate error on the fitting function we were able to quantify our diameter error. This gave us a value of  $a = 0.21 \pm 0.2\mu\text{m}$ , a few standard deviations from the manufacturer's value ( $0.3\mu\text{m}$ ).

As mentioned previously, there is only a limited range of linear behaviour in figure 5. A couple of DLS' limitations are likely causing this. Firstly, the time taken for the signal to decay can either be too large, such that during the 10 s we were recording the signal had not significantly decayed, or too small, such that within a very small number of samples the decay had dropped substantially. Both of these would make fitting any realistic exponential decay impossible. The limiting  $q$  values can be roughly calculated as the follows:

$$q_{max} \approx \sqrt{\frac{1}{\tau_{OneReading}D}} \quad q_{min} \approx \sqrt{\frac{1}{\tau_{EntireReading}D}}$$

We have followed the logic that a signal must either have decayed by  $e^{-1}$  within the time over which we recorded, for minimum  $q$ , or not have decayed by  $e^{-1}$  before a second reading has been taken, for maximum  $q$ , in order to be accurately fitted. This calculation tells us that for the high

q limit the limiting angle was roughly 160 degrees for low q was about a degree. Both of these are significantly beyond our extremal measured angles.

What then is causing our non-linear behaviour at high and low angle? The laser has a finite angular width and at low angles some of the unscattered laser beam is likely registering at the detector, this is pushing up our low q limit to angles of roughly 5 degrees, beyond which the noise from the laser is no longer the dominant factor. On the other hand, at large angles the intensity of scattered light becomes very low, perhaps lower than the background noise level despite our best efforts to minimise this. Our largest angle used was about 30 degrees, beyond which the intensity of scattered light is too low to be reliably measured.

## 3 Differential Dynamic Microscopy

### 3.1 Theoretical Background and Methodology

We shall now describe the main focus of this project, Differential Dynamic Microscopy (DDM), a relatively new development [2]. Thanks to the advent of large amounts of commercially available computing power we are able to Fourier transform the signal directly rather than letting optics do it for us. While requiring large amounts of computation this has the advantage that one video can be used to find the behaviour at a very large range of  $q$  values, performing days of experiments in minutes.

Hence the protocol progresses as follows. A slide containing a small amount of liquid laced with tracer particles is placed in the path of a laser of arbitrary wavelength. The slide is then imaged through an objective using a digital camera.

A comparison function between frames is then calculated,  $I(q, \tau)$ , the equivalent of the auto-correlation in DLS. The pixel values of one frame at a time  $t$  plus some lag time  $\tau$  are subtracted another at time  $t$  and to produce a pattern which will reflect only differences between the two frames. Videos containing potentially thousands of frames, each of about a million pixels, make subtracting every frame from every other a lengthy process; instead only 100 or so randomly selected comparisons were made for each lag time, which were then averaged over, although this parameter (number of couples) can be manually varied.

This comparison is then averaged radially before being Fast Fourier Transformed. Our image is two dimensional so we could theoretically calculate a  $q_x$  and  $q_y$ , but we would expect the distribution to be isotropic and hence the two would be identical. We can therefore reduce computation time by averaging radially and treating the system as one dimensional.

$I(q, \tau)$  would begin at 0 intensity when  $\tau$ , the lag time, was 0, as after no time has passed the two frames will be exactly the same. At large lag times the images will be completely randomised by the movement of particles causing  $I(q, \tau)$  to plateau. In between these two limits it will exponentially approach the plateau. Therefore we fit each Fourier mode with a function of the form:

$$h(q, \tau) = A(q)[1 - e^{-\frac{\tau}{\tau_c}}] + B(q)$$

Where  $\tau_c$  is the same decay constant of structure in a sample of particles undergoing Brownian Motion:

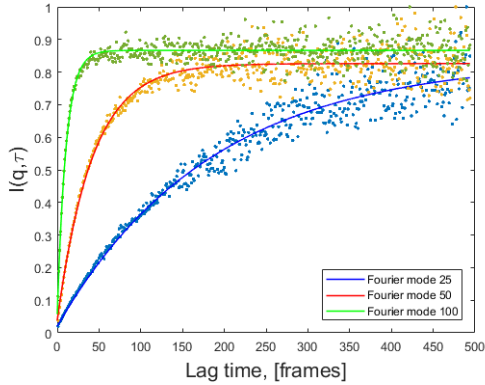
$$\tau_c = \frac{1}{Dq^2}$$

In summary, by fitting the curve to each Fourier mode's  $I(q, \tau)$  we can find the characteristic decay time. This can then be used to calculate features of the particle or fluid under consideration. Serendipitously it is not important to have the particles perfectly focused, a small airy disc of a particle out of focus will produce the same result as a perfectly focused point, hence the non-negligible  $z$  axis height can be ignored and the system taken as two dimensional. In addition, fixed defects, such as dust, do not have an effect on important quantities, as we are only using data produced by the difference between two frames, removing stationary defects.

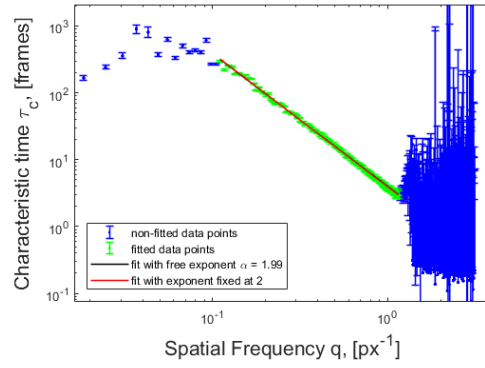
### 3.2 Comparison With DLS

Our first test of the equipment, and a useful showcase of the details of the technique, was a run with the same  $0.3 \mu\text{m}$  particles we used in the DLS. As suggested each mode can be seen in figure 6a to decay with a different decay constant.

When the decay time is plotted as a function of Fourier mode on a log-log plot only a region is seen to be linear, as in DLS (figure 6b). Glossing over the limited linear region for a moment, a fit of a graph with gradient -2 onto this data produces a straight line with an intercept that can be used to find the particle size. Values of  $D_{exp} = 1.34 \pm 0.01 \mu\text{m}^2\text{s}^{-1}$  and  $Diameter_{exp} = 0.321 \pm 0.003 \mu\text{m}$  were found where the expected values were  $D_{theo} = 1.43 \mu\text{m}^2\text{s}^{-1}$  and  $Diameter_{theo} = 0.3 \mu\text{m}$ . The theoretical values are therefore more than two standard deviations from the experimental ones. On the one hand, this suggests something must be going amiss, my guess would be the edge effects of the glass slide changing the diffusion of the particles. On the other hand, these error bars arise from the error in the fitting function, which takes no account of the error on the points to which it is fitting. This means the error could be considerably larger, perhaps to such an extent that the results became consistent. Regardless, this is much more accurate than the DLS value.



(a) The intensity of  $I(q, \tau)$  vs  $\tau$  for three different  $q$  values, labelled as Fourier modes.



(b) Log-log graph of time constant against wavevector,  $q$ . Two lines, one of free gradient and one with a gradient -2 have been fitted to the linear region. In this case the two agree very well. From the intercept we can calculate  $D$  and hence the quantities of interest.

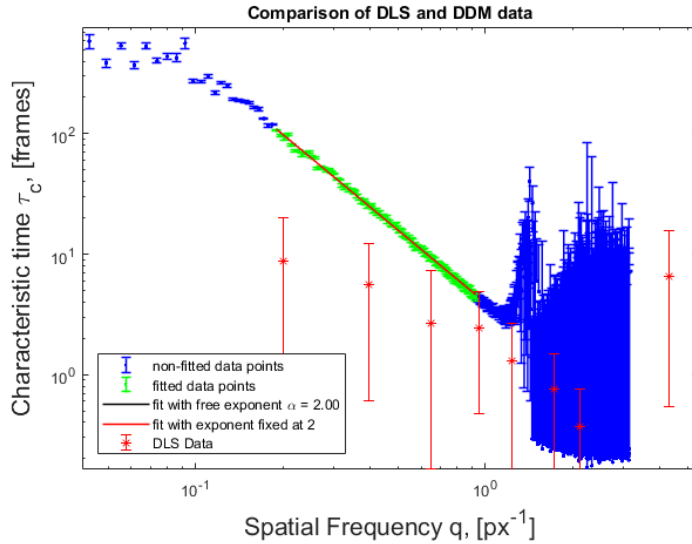


Figure 7: DLS and DDM data for the same scattering sample plotted on top of each other. Notice for example the systematic difference.

When the DDM and DLS datasets are plotted on the same axes some very interesting features are noted (figure 7). Firstly, there appears to be a systematic difference between the data sets. In fact, the factor that relates the fit on the DLS data with the fit on the DDM data is  $\approx 1.5$ , roughly the factor by which the DLS radius estimate is too small. Secondly, the linear regions of the two techniques are different, DLS' large and small  $q$  limits are both higher than DDM's. This and other such features shall be explored in the next section.

### 3.3 Tuning Experimental Parameters and Examining Linear Boundaries

#### 3.3.1 High $q$ Linear Limit

The first factor that could place high  $q$  bounds on the linear region is the frame rate. At very short wavelengths the system may have decorrelated in only a couple of frames before the camera has time to make measurements, making fitting impossible. The camera we used ran, at most, at 100 frames per second. We tested how the  $q$  limit changed with changing frame rate. In order to do this we actually did not record separate videos but simulated a lower frame rate by only analysing 1 in 2 (or other integer as appropriate) of the frames from a particular video. In this way all other parameters were guaranteed to be identical. This method only allowed us to analyse frame rates

that were integer divisions of 100 fps, but this sufficed for a rough overview.

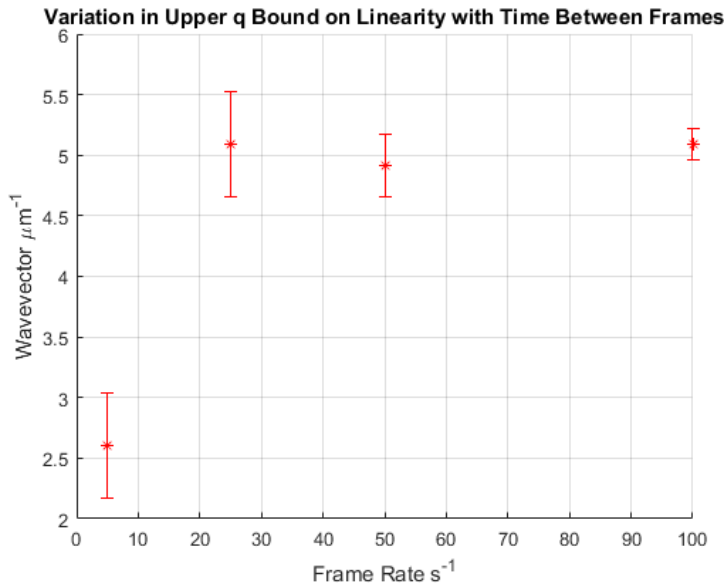


Figure 8: As can be seen there appears to be another constraining factor at high frame rate, only at very low levels does the boundary begin dropping.

As can be seen from figure 8, taken at 20x magnification, the frame rate does not appear to be the limiting factor until we reach rates of a few frames per second. The  $q$  is capped at roughly  $5 \mu m^{-1}$  at the high frame rates. A theoretical basis for this can be found through a rough calculation. In a system where the frame rate is the limiting factor we might expect the smallest wavelength that can be recorded to be roughly:

$$q_{max} \approx \sqrt{\frac{1}{\tau D}}$$

Where the time  $\tau$  is the time between frames, i.e. the inverse of the frame rate. This is justified in a similar manner to before, it roughly represents the highest  $q$  for which the signal is still visible after one frame. The precise factors in this model are not certain - would the fit be possible if the exponential had dropped to 20% after one frame? Or 10% or 50%? It is hard to say. The above calculation assumes that the limit is placed by a  $e^{-1}$  decay within one frame. Our system appears to be limited at  $5 \mu m^{-1}$  regardless of frame rate, we can ask what the minimum frame rate we could run at without further constraining the system? The calculation tells us this would be 35 fps. This is roughly what is seen in figure 8 to within a factor of 2 or so. Suffice to say that it appears that our theoretical model is roughly correct and that at reasonable frame rates there is no constraint on high  $q$  due to limited temporal resolution.

What else could then constrain  $q$ ? If not temporal resolution it could be spatial. The pixel size defines the spatial resolution and this changes depending on which objective is used. If the spatial sampling frequency is lower than the Nyquist frequency (twice the signal frequency) the signal will not be accurately measured, but aliased. We tested the change in high  $q$  limit with objective and the results are shown in table 1.

Objective	10x	20x	40x
Numerical Aperture	0.25	0.3	0.65
High $q$ Limit ( $\mu m^{-1}$ )	$4.8 \pm 0.2$	$5.1 \pm 0.2$	$8.3 \pm 0.4$
Theoretical NA Limit ( $\mu m^{-1}$ )	2.5	3.0	6.4

Table 1: Table showing the change in high  $q$  limit with objective.

As observed there is a change, but it does not appear to follow objective. If this limit was due to spatial sampling below the Nyquist frequency it should double with each objective doubling. Rather perhaps this is a result of the changing numerical aperture (NA). The smaller the NA the

smaller the largest angle that is admitted by the lens and hence the smaller the smallest wavelength Fourier Modes present in the image, limiting resolution. The resolution is related to NA as follows:

$$Resolution = \frac{\lambda}{2NA}$$

This places a resolution limit a few times higher than the pixel size. Hence:

$$q_{max} = \frac{\pi}{Resolution} = \frac{2NA\pi}{\lambda}$$

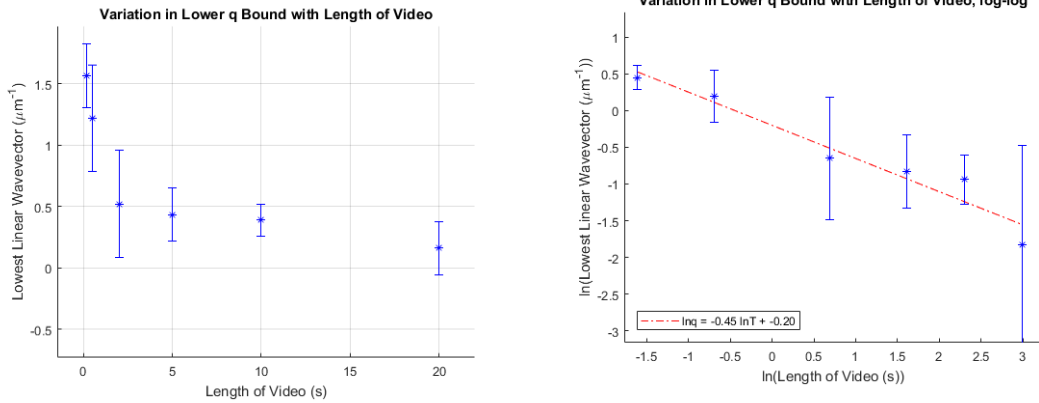
This prediction can be seen in table 1 and scales in roughly the correct manner, however seems a factor or so off, which is reasonable considering the coarseness of our analysis. Various different formulae for the resolution limit due to NA are used, it is not a fixed border but a fuzzy boundary. Perhaps our system works right up to the edge of this fuzzy boundary.

To compare this to the last section, DLS does not suffer from the same limited spatial resolution or numerical aperture problems as DDM. Hence its high  $q$  mode at  $\theta \approx 30^\circ$  is at a larger angle than the DDM's most highly scattered fitted mode at 20x magnification. This means that the linear region in DLS will have a higher  $q_{max}$  as in figure 7.

### 3.3.2 Low $q$ Linear Limit

At low  $q$  our choices for limiting factor become, one, do we have enough time to observe the decay? Or two, is the field of view large enough to see the largest wavelengths?

We tested videos of various lengths between 20s and 0.2s at 100 fps. Again we used the same video truncated at different points to keep all other parameters constant. This was performed at 20x magnification and the data is shown in figure 9a:



(a) The change in linear  $q$  lower bound with video length

(b) Log-log plot of the change in linear  $q$  lower bound with video length. Line of best fit is  $\ln q = -0.45 \ln T - 0.20$ , very close to that predicted.

Figure 9: Plots showing the effect of total video length on linear  $q$  low bound.

It appears that it is indeed length of video limiting us. In particular, we notice the line of gradient  $-0.5$  on the log log graph (figure 9b). A similar calculation to those previously performed can justify this. We would expect that a mode must have decayed by roughly  $e^{-1}$  during the video in order to be accurately fitted, placing a minimum on the viable  $q$  values. This minimum should behave as follows:

$$\ln q = -\frac{1}{2} \ln \tau + \frac{1}{2} \ln \frac{1}{D} = -\frac{1}{2} \ln \tau - 0.19$$

Which is almost exactly observed.

The other factor that could be constraining the linear region would be the field of view size. Periodicities larger than the field of view would be difficult to observe in the fourier transform. The field of view scales with objective so we tested how the minimum  $q$  changes with objective, the results are shown in table 2.

Objective	10x	20x	40x
Numerical Aperture	0.25	0.3	0.65
Low q Limit ( $\mu m^{-1}$ )	$0.28 \pm 0.07$	$0.4 \pm 0.3$	$0.7 \pm 0.13$

Table 2: Table showing the change in low q limit with objective.

It appears that this too is constraining us, as we decrease the field of view the q minimum increases. The data suggests that the wavelength must be about 10 times smaller than the dimensions of the field of view in order to be measurable. A couple of details about this confuse us. Firstly, how could two factors be simultaneously constraining us? Surely the more constraining factor always wins out. This is only consistent if the two factors coincidentally limit us to the same value, which is surely unlikely? Secondly, why must the wavelength be an order of magnitude smaller than the field of view in order to be visible? The exact factors here are confusing, for example we radially averaged which you would expect to change the dimensions slightly. Nonetheless the question of what is the smallest periodicity present in a sample of finite length is one I have not satisfactorily answered.

With reference to the DLS, the non-scattered laser light limits our linear region to angles greater than  $5^\circ$ . This corresponds to a spatial frequency of  $1.15 \mu m^{-1}$ , plenty larger than the DDM limit. It therefore makes sense that the low end linear limit for DLS is much higher than that of DDM as in figure 7.

### 3.3.3 Particle Concentration

The more particles the more light is scattered, but the less light is able to pass through the medium. The concentration of particles is therefore a compromise between an opaque solution that doesn't let light pass and plain water with minimal scattering. We therefore tested a range of feasible concentrations for particles of known diameter ( $0.865 \mu m$ ), table 3.

Concentration (by Solid Mass)	$D_{Experimental}$ ( $\mu m s^{-1}$ )	Diameter ( $\mu m$ )
0.1%	$0.46 \pm 0.01$	$0.94 \pm 0.1$
0.05%	$0.48 \pm 0.01$	$0.90 \pm 0.1$
0.025%	$0.52 \pm 0.01$	$0.83 \pm 0.1$
0.01%	$0.50 \pm 0.01$	$0.86 \pm 0.1$

Table 3: DDM Analysis Results for Different Concentrations of  $0.865 \mu m$  Polystyrene Beads.  $D_{Theoretical}$  is  $0.50 \mu m s^{-1}$

Within our range of concentrations the results are roughly correct. In addition, there is no correlation between concentration and the variations from the correct answers. We analysed both the high and low q limits and the error on each sample and this too did not change noticeably with concentration. This suggests that within this range the setup works sufficiently well not to worry too much about concentration effects.

### 3.3.4 Number of Couples

As discussed it is possible to change the number of couples used to calculate  $I(q, \tau)$ . We tried varying this, and observed no significant effect on the predicted diameter or the high q or low q boundaries. The only thing that did change was a decrease in the error of the fitting function within the linear region, a representative example is shown in table 4. Since each addition of frames markedly increased computing time, and the error at 100 couples was manageable, we left this at 100.

Number of Couples	100	200	400
Diameter Error (nm)	3	2	0.2
Fitting Error (a.u.)	0.61	0.57	0.52

Table 4: Variation in error on diameter and on a representative fitted parameter as the number of couples is changed.

### 3.4 Effects of Changing Particle Size

We used a variety of polystyrene beads with diameters between 0.3 and 1  $\mu\text{m}$ . The high and low  $q$  limits remained constant, as predicted by such a resolution limited system. The error on the other hand varied considerably. Firstly, all the estimates of particle radii were too large. Secondly the errors generally became larger the larger the particle radii. Most are tolerably mistaken, but the largest particle has a prediction over an order of magnitude larger, as shown in table 5.

Particle Diameter ( $\mu\text{m}$ )	0.3	0.6	0.865	1
Error (no units)	0.61	0.69	1.166	4.4
Experimental Diameter ( $\mu\text{m}$ )	$0.321 \pm 0.003$	0.72	0.93	19

Table 5: Table showing experimentally derived diameter and the error on a representative fitting parameter for one  $q$  value for each particle. N.B. the error is not the error on the particle size, but a representative example of fitting error.

The assumption we have been making thus far is that the densities of polystyrene and water are equal, thus the particles float unimpeded and we can treat it as a 3D Brownian Diffusion. In fact  $\rho_{polystyrene} = 1.04\text{gcm}^{-2}$  while  $\rho_{water} = 1.00\text{gcm}^{-2}$ . This will have an increasing effect as the particle gets larger, so perhaps these particles were in fact undergoing 2D diffusion on the bottom of the slide (we discuss this further in section 4.3). Why there is such a sudden difference between the quality of answer I can't say, my only thoughts are a) we may have left the 1 $\mu\text{m}$  slide untouched for longer allowing the particles to more comprehensively settle b) the beads may actually not be polystyrene but I just failed to note this.

## 4 Further Experimentation Using DDM

Now that we have satisfactorily tested the setup we shall present some examples of further experimentation.

### 4.1 Viscoelastic Fluids

A fluid can resist motion in more than one way. A purely viscous fluid will exert a force proportional to the velocity of the moving particle, i.e. if the particle is oscillating this force will be  $\frac{\pi}{2}$  out of phase. An elastic medium on the other hand will try and restore a particle to some equilibrium position, like a spring, exerting a force in antiphase with the displacement. Viscoelastic fluids can display a mixture of these two behaviours, and this can be encoded in a complex modulus of the material, which in general we would expect to be a function of frequency.

$$G^*(\omega) = G'(\omega) + iG''(\omega)$$

Microrheology uses the seeding of a fluid with tracer particles to measure fluid properties. It can be shown that [3]:

$$G^*(\omega) = \frac{k_b T}{\pi a s \langle \Delta x^2 \rangle} \Big|_{s=i\omega}$$

Where  $\langle \Delta x^2 \rangle$  is the Laplacian transform of the Mean Squared Displacement (MSD) of the tracer particles. Various methods can be used to find this, however DDM presents an obvious solution.

#### 4.1.1 Glycerol

We first tested this on Glycerol at various concentrations, a purely viscous fluid. As predicted  $G''$  was linear with frequency, seen in a characteristic figure 10. Since the fluid was purely viscous we used the same techniques as before to calculate a value for  $D_{exp}$  and from this the viscosity of the sample. The results of which are shown in table 6, and are broadly similar to the data book values.

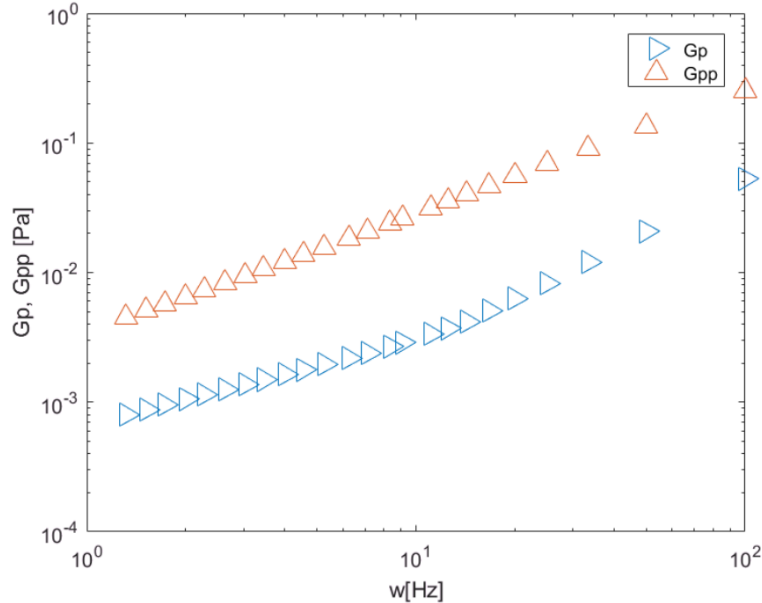


Figure 10: Graph of  $G'$  ( $G_p$ ) and  $G''$  ( $G_{pp}$ ) against frequency for a characteristic glycerol trial (82.7% glycerol). The behaviour of  $G'$  in this region doesn't carry much information, as the linear  $G''$  shows us that the fluid is viscous. The  $G'$  line is probably mainly spurious.

In these viscous fluids  $G'$  should be zero; from figure 10 it appears that this is not the case. What should perhaps be considered is that  $G'$  is an order of magnitude smaller than  $G''$  and could well represent a very small spurious output from our analysis.

Percentage Glycerol	0%	48.8%	82.7%	97.5%
$\eta_{Exp}$ (mPas)	1.1	7.4	104	650
$\eta_{DataBook}$ (mPas)	$0.914 \pm 0.01$	$4.9 \pm 0.05$	$69.2 \pm 0.7$	$702 \pm 50$

Table 6: Experimentally derived viscosities for varying calculations of Glycerol

### 4.1.2 Polyethylene Glycol

Our next test was on a truly viscoelastic fluid. Polyethylene Glycol (PEO) forms long chains that constrain the particles, resisting displacements like the springs in an oscillator, as well as offering viscous resistance. We used a solution of 2% PEO and were careful to give it time to come to rest both when the sample was originally mixed, to ensure the tracer particles were comprehensively integrated into the fluid, and again when it was placed on a slide.

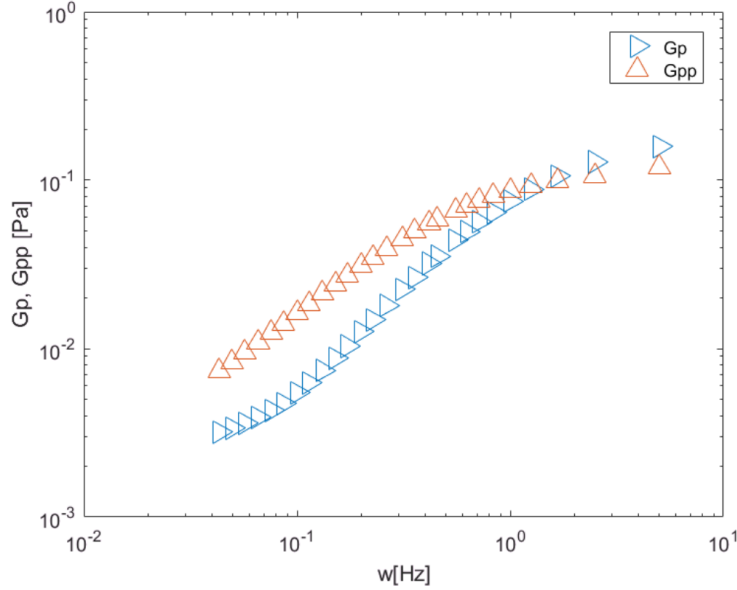


Figure 11:  $G''$  and  $G'$  against frequency for the viscoelastic polymer PEO

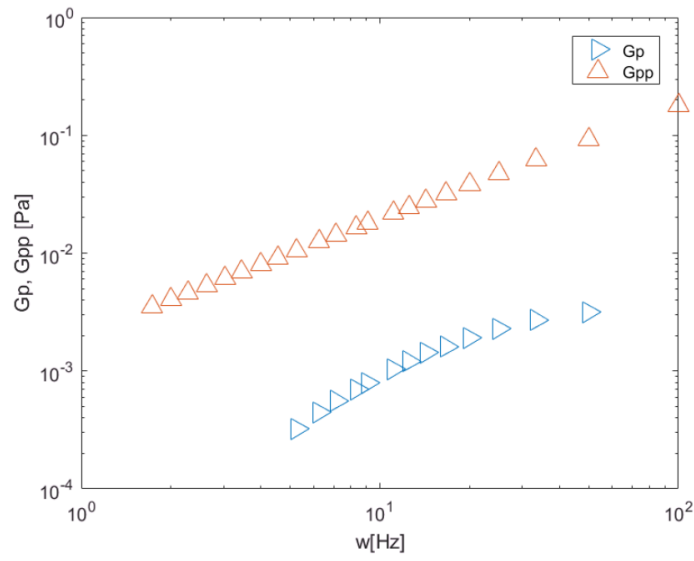
Figure 11 shows the measured  $G'$  and  $G''$  behaviour. This material is clearly no longer merely viscous, i.e. the  $\ln(G')$  is not linear with frequency and the magnitude of  $G''$  is comparable to that of  $G'$ , especially at the higher frequencies. Previous literature on the topic [3] produced a very similar graph to this.

### 4.1.3 Pluronics

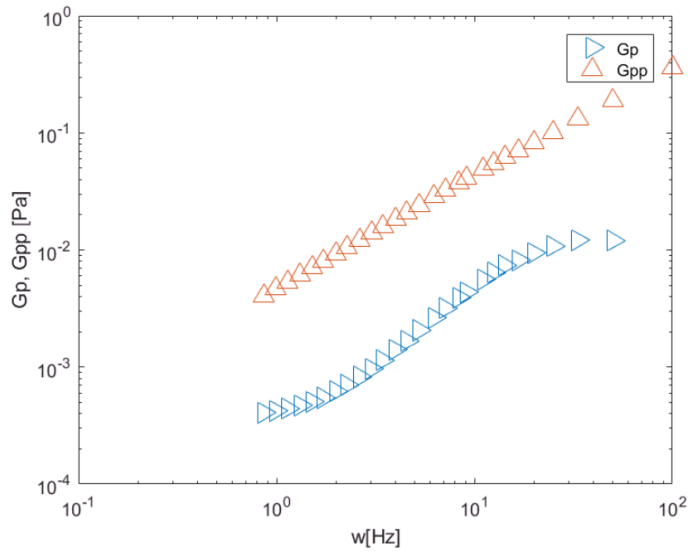
Finally we tested another viscoelastic fluid. Pluronics are surfactants and as such possess hydrophobic/philic ends. These form vesicles that can act to constrain the particle, again giving the complex modulus a significant elastic component, as long as the concentration of pluronics is high enough. Three concentrations were tested and their  $G^*$  behaviour is shown in figure 12.

We can see here the fluids appear viscous at low concentrations, showing the linear  $G'$  and spurious  $G''$  characteristics that first made an appearance in our example Glycerol run (figure 10). For 5% we measure a viscosity of 2.4 mPa s and 10% of 6.2 mPa s. The 20% solution however displays some elastic behaviours at high frequencies; at roughly 1Hz  $G''$  becomes nonlinear. Previous literature on the topic [4] predicts a roughly similar pattern, even down to the frequency at which the nonlinearity begins. Beyond this it is hard to tell how much the data agrees with the finding of Ranieri et al., as the exact concentrations used by our two experiments differ. The general shape appears to be in agreement. The numerical values on the hand are inconsistent. Ours tend to be smaller, often wildly so. Our 20%  $G'$  for example is many orders of magnitude smaller than Ranieri et al.'s.

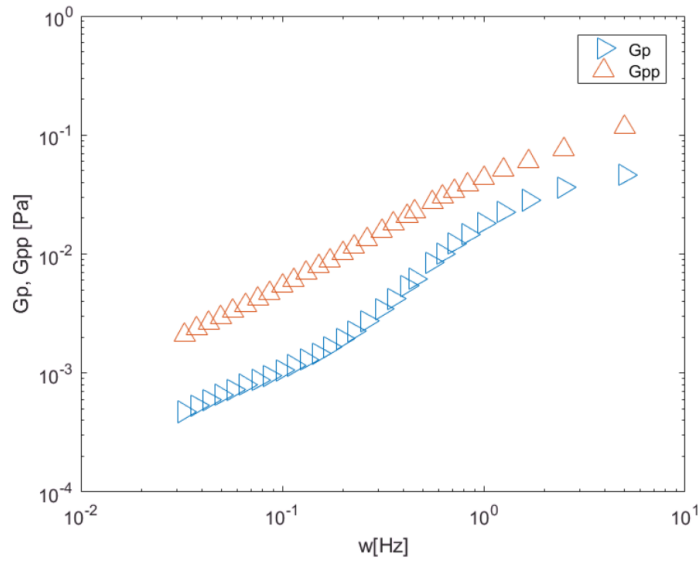
Many factors could have caused this. As the tracers move less in these more viscous sample we are forced to use longer videos, which are more prone to being vibrated as people walk around or



(a) Behaviour at 5% concentration.



(b) Behaviour at 10% concentration.



(c) Behaviour at 20% Concentration

Figure 12: The variation of  $G'$  and  $G''$  for a Pluronic solution at three different concentrations

touch the table. These vibrations make the video next to useless if they are large, and, though we tried to minimise this, residual vibrations could be present. In addition, we attempted to give all samples enough time to fully mix and settle when placed on the slide. There was however only a couple of days leeway and as such our resting times were an order of magnitude smaller than those used by Ranieri et al. Perhaps this is having effects?

## 4.2 Ballistic Motion of Particles

To examine the effects of gravity on the diffusion of silica particles (heavier than water) we tilted the setup at 90 degrees. The particles then flow downwards and eventually settle at a terminal falling velocity in addition to the pre-existing diffusive flow. With particles this small both effects are important and it can be shown that a fitting of the type:

$$h(q, \tau) = A(q)[1 - e^{-Dq^2\tau} \text{sinc}(qv\tau)] + B(q)$$

is more appropriate, where  $v$  is the terminal velocity of the particles. This fitted well within a small  $q$  range, as shown in figure 13.

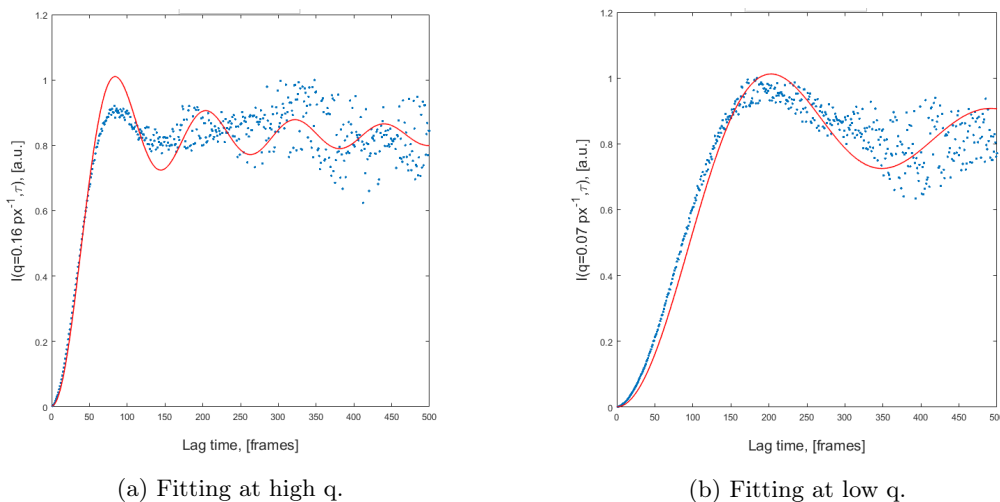


Figure 13: Examples of the sinc ballistic fit at different  $q$  values.

From these fits it was possible to find a value for the terminal velocity of the particles.

Using Stokes' formula for the force on a sphere flowing through viscous fluid, and the buoyancy force, it is possible to theoretically calculate a value for the terminal velocity:

$$\frac{4}{3}\pi g a^3 (\rho_{silica} - \rho_{water}) = 6\pi a \rho v$$

$$v = \frac{2ga^2(\rho_{silica} - \rho_{water})}{9\eta}$$

Where  $\rho$  represents the densities,  $a$  the radius of the particle,  $\eta$  the viscosity of water and  $g$  the acceleration due to gravity. The first equation follows from the net zero balance at terminal velocity of buoyancy, weight and drag. The results are shown in table 7.

Particle Diameter	3.47 $\mu\text{m}$	1.5 $\mu\text{m}$
Experimental velocity	7.9 $\mu\text{m}\text{s}^{-1}$	8.0 $\mu\text{m}\text{s}^{-1}$
Theoretical velocity	43 $\mu\text{m}\text{s}^{-1}$	8.1 $\mu\text{m}\text{s}^{-1}$

Table 7: Comparison of Experimental and Theoretical terminal velocities of Silica Particles falling under gravity.

As can be seen for the 1.5 $\mu\text{m}$  particle these results are remarkably close, vindicating the method. The 3.47 $\mu\text{m}$  particle on the other hand likely suffers to a much larger degree from edge effects, something we shall now move on to discuss.

### 4.3 2D Diffusion of Heavy Silica

As discussed above silica is denser than water and hence will fall. Even on the very thin slide this means that after leaving it for a small amount of time the silica will sediment. If we then image the behaviour in this stable state we would expect two, rather than three, dimensional diffusion on the glass surface. This, we would expect, to have different characteristics.

A first test of this would be to assume the diffusion was still three dimensional and see if the model fits. For silica beads of diameter  $3.47\mu\text{m}$  a  $D_{exp}$  value of  $0.05\mu\text{ms}^{-1}$  and hence calculated diameter of  $8.6\mu\text{m}$  is recorded, theoretically we would expect  $D_{theo}$  to be  $0.124\mu\text{ms}^{-1}$ . This strongly suggests our model is wrong.

Where to go from here? One thing to change might be the Stokes' approximation we have used to calculate the D value. Oseem's equations give a next order correction to the factor  $\zeta$  in terms of the Reynolds Number, Re.

$$Force = 6\pi\eta a(1 + \frac{3}{8}Re)$$

If we can then only find a way to calculate the Reynolds number we might be able to develop a better fitting model, though I was stumped as to how to do this.

### 4.4 Particle Mixtures

A mixture of two particles should also be amenable to DDM analysis, to the extent that features such as relative effective scattering area should be calculable if the concentrations are known. The only feature that has to change is the fitting function, which now becomes:

$$g(q, \tau) = A(q)[1 - e^{-\frac{\tau}{\tau_{c1}}}] + B(q)[1 - e^{-\frac{\tau}{\tau_{c2}}}] + C(q)$$

Where  $\tau_{c1}$  and  $\tau_{c2}$  are the two decay constants of each particle.

We performed a run containing  $3.47\mu\text{m}$  Silica and  $0.3\mu\text{m}$  Polystyrene beads. These were chosen to maximise the diameter difference and hence the decay time difference, even if it meant we had to use the sinking Silica beads. In fact the sinking of the Silica beads helps us, as Silica's effective diameter in this model is larger, by roughly a factor of 2.5, than you would expect. This is due to its confined 2D diffusional behaviour as discussed in section 4.3.

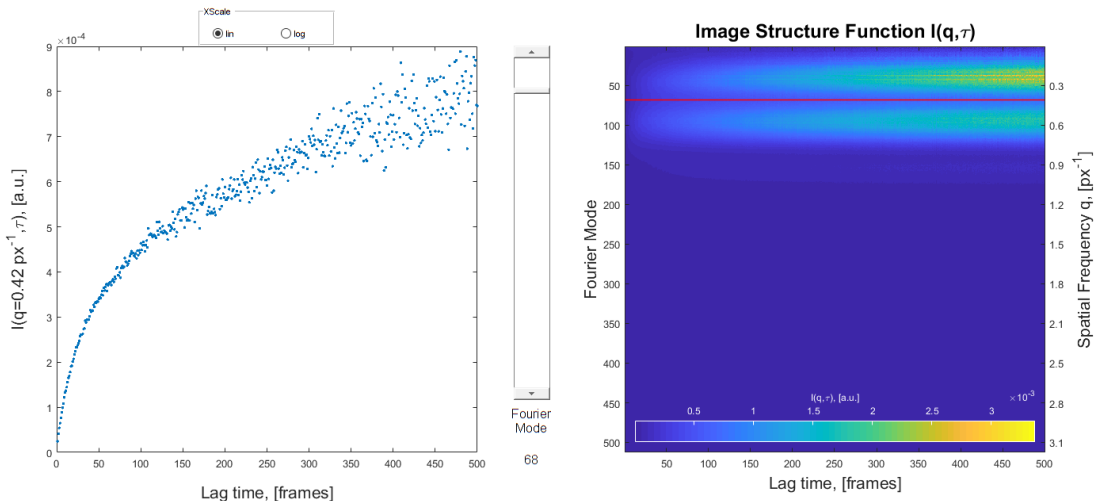


Figure 14: On the left is the comparison function,  $I(q, \tau)$  for one particular Fourier mode, by eye it appears to contain two separate decays. The image structure function on the right shows the intensity of  $I(q, \tau)$  at each mode after a lag time  $\tau$ . Notice the clear bimodal characteristics.

Figure 14 shows  $I(q, \tau)$  for this two particle mix. The key detail of note is the bimodal intensity bands. While this does represent structure in the increasingly uncorrelated regime of the comparison function it still seems indicative of the two particle mix.

We fell into problems when trying to fit the double exponential. The fit was very dependent on the starting parameters suggesting it was falling into local rather than global minima. The

two exponentials likely had a decay constant that was too similar, causing the analysis to fit one exponential with a much larger coefficient, encompassing large parts of the behaviour, followed by a second, much more minimal, correction.

While this is not ideal, in this case, where the particle diameters are so different, the analysis threw up some interesting results. The time constant from the major exponential fit featured two 'humps' each with a linear region when plotted against  $q$ , figure 15. When each of these linear regions is separately used to calculate a particle radius we retrieve values of  $8.7 \mu\text{m}$  and  $0.32 \mu\text{m}$ , impressively close to the 'effective' silica diameter and real Polystyrene diameter of  $8.6 \mu\text{m}$  and  $0.3 \mu\text{m}$ .

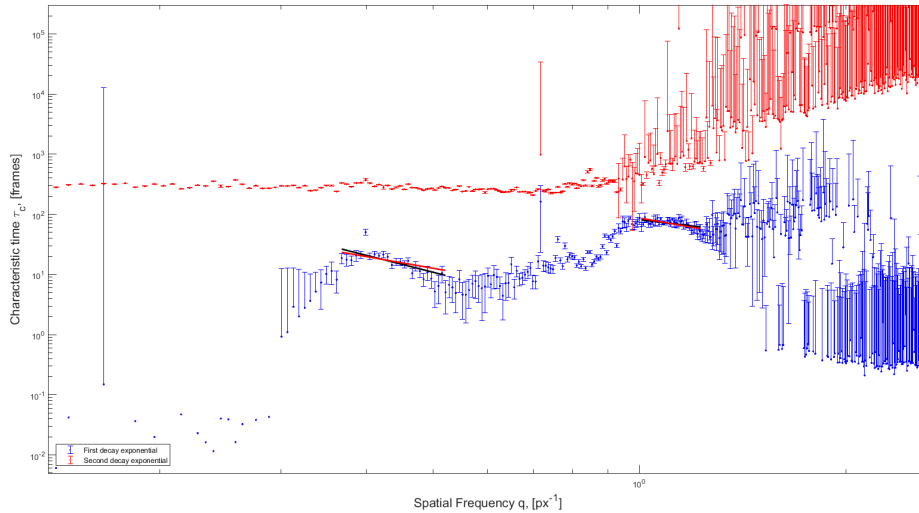


Figure 15: The two exponents of the fitting function for a two particle mixture as  $q$  varies. Included are lines of gradient -2 on the two linear regions (the free parameter fits had gradients of 2.8 and 1.3) which were used to calculate the particle sizes. The red data represents the minor exponent which likely carries little extractable information or meaning.

#### 4.5 Finding Temperature Dependence of Viscosity

A brief attempt was made to find the viscosity of water as a function of temperature. However, the data was terrible, barely varying from the room temperature value of  $10^{-3} \text{Pas}$ . This was probably due to a poor temperature control system, our water bath was just a beaker and cooled very quickly. In theory however this would be an easy application of DDM had we used a larger, more consistent water bath and left the slide in for longer so that it reached thermal equilibrium.

## 5 Conclusion

In conclusion we have tested two techniques for analysing the scattering of light by spherical tracer particles undergoing Brownian Motion: Dynamic Light Scattering and Differential Dynamic Microscopy. The two were compared; for a test particle of diameter  $0.3 \mu\text{m}$  DLS and DDM reported figures of  $2.1 \pm 0.2 \mu\text{m}$  and  $3.21 \pm 0.003 \mu\text{m}$  respectively. The limitations of each technique, in particular the limits of the  $q$  region over which our model held, were comprehensively probed, and the dependence of these limits on various parameters were tested.

We then proceeded to apply DDM to a variety of other situations. The complex moduli of a series of viscous and viscoelastic fluids were found and the technique proved proficient at this. We then examined the ballistic motion of particles under gravity providing satisfactory estimates of the terminal velocity for one particle size, the other being larger and limited by edge effects. The behaviour of this larger particle was examined and appeared to be some form of 2D diffusion that we failed to model. A two particle mix was analysed and, despite analytic failures, satisfactory estimates of both particle sizes were found from only one video.

Opportunities abound for further work in almost every area our experiment touched. Larger ranges on the parameters we varied (such as objective or numerical aperture) would allow us to better assign the linear regime of both DLS and DDM. A deeper analysis of why the particle diameter was consistently overestimated by DDM seems imperative, and could well give us more details about the diffusive behaviour of the particles when constrained in the slide.

The theory behind viscoelastic fluids is deeper than I have been able to dive, however DDM seems a potentially extremely useful addition to the arsenal of microrheology. Its key advantage is the speed with which a vast range of frequencies are tested, and there are certainly plenty of fluids waiting to be tested. The 2D diffusion of heavy silica must be an area amenable to DDM if only the correct analysis was applied. Despite this setback we were able to find some accurate results using a mixture containing the same heavy silica and some polystyrene beads. It is possible to extract meaningful data from these videos; our analytics could be markedly improved, but this problem is definitely tractable. Finally, our attempt at viscosity measurement can definitely be repeated and improved.

Beyond deficits in our own experimentation the larger possibilities are exciting. Other groups have previously used DDM to study bacterial motion[5][6], anisotropic colloid distributions[7] or aggregation processes[8]. The most exciting of these to me seems to be the application to biological motion, if it works with bacteria why not larger organisms? The popular model organism *C. elegans* has had its motion extensively studied in order to examine motor patterns and their production. However collecting worm movement data is currently fairly painstaking, progressing worm by worm. If instead we analysed a bulk of hundreds of worms using DDM, quicker, much more accurate, analysis of characteristic motions would be possible.

Differential Dynamic Microscopy represents an impressive application of mathematical modelling to study a highly probabilistic process. Thanks to the advent of large amounts of computing power it is now surely the foremost technique for the study of not just colloidal systems but any such small scale scattering system.

## References

- [1] Bruce J. Berne and Robert Pecora, *Dynamic Light Scattering*, John Wiley and Sons, Inc., 1976.
- [2] Roberto Cerbino and Veronique Trappe, *Differential Dynamic Microscopy: Probing Wave Vector Dependent Dynamics with a Microscope*, Phys. Rev. Lett. 100, 188102, Published 5 May 2008
- [3] Paolo Edera, Davide Bergamini, Veronique Trappe, Fabio Giavazzi, and Roberto Cerbino, *Differential Dynamic Microscopy microrheology of soft materials: a tracking-free determination of the frequency-dependent loss and storage moduli*, arXiv: <https://arxiv.org/abs/1708.07170>
- [4] Filipe E. Antunes, Luigi Gentile, Cesare Oliviero Rossi, Lorena Tavano, Giuseppe Antonio Ranieri, *Gels of Pluronic F127 and nonionic surfactants from rheological characterization to controlled drug permeation*, Colloids and Surfaces B: Biointerfaces, Published 6 May 2011
- [5] L. G. Wilson, V. A. Martinez, J. Schwarz-Linek, J. Tailleur, G. Bryant, P. N. Pusey, and W. C. K. Poon, *Differential Dynamic Microscopy of Bacterial Motility*, Physical Review Letters 106, 018101, Published 5 January 2011
- [6] Vincent A. Martinez, Rut Besseling, Ottavio A. Croze, Julien Tailleur, Mathias Reufer, Jana Schwarz-Linek, Laurence G. Wilson, Martin A. Bees, Wilson C. K. Poon, *Differential Dynamic Microscopy: a High-Throughput Method for Characterizing the Motility of Microorganism*, Biophysical Journal, Volume 103, 1637-1647, 8 February 2012
- [7] Mathias Reufer, Vincent A. Martinez, Peter Schurtenberger, and Wilson C. K. Poon, *Differential Dynamic Microscopy for Anisotropic Colloidal Dynamics*, Langmuir, 2012, 28 (10), pp 4618–4624, February 10, 2012
- [8] F. Ferri, A. D'Angelo, M. Lee, A. Lotti, M. C. Pigazzini, K. Singh, R. Cerbino, *Kinetics of colloidal fractal aggregation by differential dynamic microscopy*, The European Physical Journal Special Topics, Volume 199, Issue 1, pp 139–148 7 December 2011